Some views on the construction of bio-tribo-corrosion maps for Ti in Hanks solution: particle concentration and applied loads effects

M.M. Stack [1], W. Huang[2], G. Wang[2] and C. Hodge [1]

[1]Department of Mechanical Engineering

University of Strathclyde

Glasgow, G1 1XJ, UK

[2]Chonqing University of Technology,

Chongqing, China

1. Introduction

Tribology of bio-implants is a major limiting issue in materials selection of the appropriate implant for the appropriate patient activity level [1]. For example, for wear of replacement hip joints, wear caused by the sliding action of the bearing surface of the femoral head against the counterface occurs in synovial fluid. Hence, the major challenge of materials scientists in replacement of such materials is to optimize the wear resistance, minimize any potential tribo-corrosion interaction and adverse biocompatibility effects caused by such interactions and reduce wherever possible any adsorption of wear debris into the surrounding tissue.

In Tribology, and in Aqueous Corrosion, various mapping methodologies[1-7] have been developed to characterize the various interactions. The wear map developed by Lim and Ashby [2] classifies the wear regimes at ambient conditions in terms of applied load and velocity, illustrating significant temperature rises and attendant corrosion reactions as a function of the tribological variables. The Pourbaix diagram[8] considers various transitions in terms of potential and pH, therefore presenting corrosion regimes as a function of the driving force of the electrochemical reaction and the hydrogen ion concentration. In tribo-corrosion, there is an extensive recent literature combing the concepts of both approaches to construct tribo-corrosion maps [2-8].

Despite such work, there has been very little work carried out until very recently[9] on the construction of tribo-corrosion maps for application to bio-tribo-corrosion environments. This is despite the fact that such maps may have significant application in optimizing materials for

specific patient activity/mass combinations, all of which are important in selection of the most appropriate material combination in total replacement joint procedures.

In studies of wear of candidate hip joint materials, it has been observed that particle concentration of wear debris can have an adverse effect on loosening of the joint, leading to osteolysis and potential revision of the replacement joint material [10]. In such cases, it is important to identify the effects of wear debris on the tribo-corrosion mechanism [12]. Assessing the effects of such particle concentrations with load is also of significance as it will indicate what dependency, if any, particle concentration has at various body masses as defined by variation of applied load.

Hence, in this paper, the effect of applied load and abrasive concentration were assessed at a range of applied loads for Ti rotating against an inert Zirconia ball, in which abrasive particles of SiC were entrained in Hanks solution. The results were used to construct micro-abrasion-corrosion maps for application to biological environments. The significance of the bio-tribo-corrosion map in identifying mechanisms of wastage and the extent of synergy between the tribological and corrosion processes is addressed in this paper.

2. Experimental Description.

Micro-abrasion tests were performed with the TE-66, micro-abrasion tester, Figure. 1 (Plint and partners (Phoenix, UK)). The details of the experimental rig are as follows. A (25.4mm ball was located between two-coaxial shafts, each carried in a support bearing, with one of the shafts driven by a variable speed DC geared motor. A batch counter was provided to measure and control the number of shaft revolutions. A peristaltic pump head was connected to the other end of the shaft and this was used for providing slurry feed to the contact. The test sample was clamped onto a platform, which was fitted to the pivoted L-shaped arm. This arm was rotated around its pivot until the sample came into contact with the ball. The load was applied by adding dead weights to a cantilever arm. It is important to note that this was not an attempt to directly simulate hip joint conditions but instead to demonstrate the application of the concept of the micro-abrasion-corrosion map to a bio-material couple, where the analogy may be made to wear in artificial hip joints. The slurry was fed to a position just above the contact point and collected in a waste tray underneath. The relatively high concentration of SiC particles was used as to accelerate the test in order to simulate transitions between possible tribo-corrosion regimes. The specification of the apparatus is shown in Table 1.

The arm, which holds the sample, could be moved horizontally in order that several tests on a single sample specimen could be carried out. (It is recognized that with this arrangement, the actual load may deviate, particularly if the specimen looses contact with the ball at higher rotational speeds, where some experimental stability may set in). The sample was then removed from the apparatus and the diameter of the resulting abrasion scars was measured with profile projector and optical microscope.

The material of the test specimens was Ti. The chemical composition and mechanical property data are given in Tables 2-3 and SEM analysis of the specimems are given in Fig 2. The counterface ball used was Zirconia, Table 4, and was selected as stated above because it provided an inert surface against which corrosion of the counterface could be measured during the micro-abrasion test. Mechanical properties of the Zircona used are given in Table 4. The Ti surfaces were ground and polished by conventional metallographic methods before testing. Following the test, the worn samples were examined by optical, scanning electron and atomic force microscopy in addition to profilometric methods.

The solution for the tests as Hanks solution and the chemical composition is given in Table 4.

The wear volume was calculated using the standard technique [9,12] for measuring the wear scar of spherical geometry i.e. the geometry of the wear scar is assumed to reproduce the spherical geometry of the ball, and the wear volume (V) may then be calculated by measuring the crater diameter (b)

$$V \approx \pi b^4 \ (64\ R)^{-1} \quad \text{For } b << R \qquad (1)$$

The corrosive slurry was stored in a container that could be agitated by means of a laboratory magnetic stirrer and was delivered to the specimen by an integral peristaltic pump. Hence, the surface of the wear scar was immersed during the test. The pH of the solution varied between 7.2-7.8

For estimating the corrosion rate, the sample was connected to the working electrode and a reference electrode was connected by capillary tube in order to make contact with the circuit. A Pt-Ti wire mesh was used as an auxiliary electrode. To ensure that all other parts were insulated, the sample was painted with electrically nonconductive paint except at the point of interaction. The clamps and plate, which hold the sample, were made of non-conducting polymer. Potential control for corrosion studies was carried out using a Gill AC electrochemical interface (ACM instruments, UK).

In this apparatus, the solution was exposed to air at room temperature, 25^{o}C. It is important to appreciate that in an electrochemical experiment, the measured current is a net quantity being the difference between the anodic and cathodic currents. For polarization experiments carried out in aerated conditions, a background cathodic current due to oxygen reduction will always be present at potentials less than equilibrium potential for this reaction which lies between -0.96 and 0.54 V (SCE). However, where the anodic currents are comparable to the background cathodic current, then the measured anodic current is too small by a constant quantity (i.e. the oxygen reduction current). It is for this reason that many electrochemical tests are carried out under de-aerated conditions. Where deaeration is not practicable, then compensation for the presence of the oxygen reduction current is carried out to extract the correct anodic currents. It should be noted, that in this case, the uncorrected data are reported for the polarization and weight change data in order to reduce errors in the construction of the micro-abrasion-corrosion map.

The sample was prepared by initially grinding the surface to 4000 um and covering the surface with an insulating paint to prevent corrosion current measurements which could be attributed to the unabraded surface.

Micro-abrasion-corrosion tests were carried out at various applied loads (0.25 – 5N) at a various constant sliding distances. The corrosion rates (Wc) during micro-abrasion corrosion were obtained from the current densities at potentials of -0.4, -0.2, 0, +0.2 V (SCE). The total mass losses due to micro-abrasion wear and corrosion (Wac) at the above potentials were measured after 30 minutes. All the mass loss values reported relate to the metallic component and negligible

3. Results

3.1 Effect of slurry concentration and applied load on the friction coefficient

The results, Fig. 4, showed that as the applied load increased, the friction coefficient showed some changes. At the lowest load, 0.25 N, the friction coefficient was highest at the lowest concentration of particles, Fig, 4(a). However, this trend tended to reverse at higher loads, Fig. 4(b-c), where the highest friction coefficients were observed at marginally higher particle concentrations i.e. at 0.05 g cm $^{-3}$. At the highest load, 1 N, the friction coefficient was highest at 0.1 g cm^{-3}.

The variation of friction coefficient at various loads was also analysed, Fig. 5. At the lowest particle concentration, Fig. 5(a), the friction coefficient was highest at the highest load, 2N, Fig. 5(a). as the particle concentration increased, the friction coefficient was highest at 2N, Fig. (b-d).

3.2 Variation of micro-abrasion-corrosion rate with applied load at various slurry concentrations

The wear volume results, Fig. 6, as a function of particle concentration and load, indicated that there were some peaks in the wear volume as a function of increasing particle concentration at each load.

The overall mass loss can be expressed as

$$W_{ac} = W_c + W_a \quad (2)$$

where

W_{ac}= Total micro-abrasion corrosion rate (calculate from mass loss measurements)

W_c = Total corrosion rate (calculated from Faraday's law)

Wa= Total abrasion rate

Comparison between the overall mass loss (which can be compared to wear volume) and the mass loss due to corrosion indicates that there is a maximum in the value of Wac as a function of load, with increasing particle concentration, Fig.7(a-d). For the lower particle concentrations, from 0.25 to 0.1 g cm^{-3}, Fig. 7(a-c), there is a reduction in corrosion contribution, Wc, at the highest loads, with no clear pattern to the values of Wa and Wc at such concentrations. However, at the highest concentrations, Fig. 7(d-e), at 0.2 and 0.25 g $cm^{-3}$the value of Wc is approximately two orders of magnitude less than those of Wa and Wac, confirming that micro-abrasion is significantly more dominant than corrosion in such conditions.

3.3 Potentiodynamic polarization data as a function of load and particle concentration

Electrochemical polarization, Fig. 8 (a-d), showed that there was a general decrease in zero current potential as particle concentration was increased at each load. There was evidence of passivation for each of the conditions. Analysis of the polarization behavior at various load showed some surprising trends, Fig. 9. There were some differences in the behavior for the various particle concentrations.

At the lowest particle concentration, Fig, 9(a), there was a kink in the passivation curve suggesting a transpassivation process. The corrosion current densities were highest at the highest loads. There appeared to be a change in behaviour at particle concentrations of 0.05 g cm^{-3} , Fig. 9(b), with the highest and lowest corrosion current densities being observed at 1 and

2N. However, at higher particle concentrations, Fig. 9(c-e), there was evidence that the highest corrosion current densities were associated with the highest loads.

3.4 Scanning Electron Microscopy of abraded surfaces

Scanning electron microscopy, Figs 10(a-b), and at 0.2 g cm^{-3} at various loads shows a circular wear scar. There was evidence of ridge formation on the surface of the wear scar, Fig. 10(b). The wear scar at 1 N, indicated evidence of wear debris over the surface, Fig. 10(c-d).

Increasing the slurry concentration at loads of 1 N, Fig. 11, demonstrated that the wear scar was more pronounced with a fairly smooth surface observed at 0.1 g cm^{-3} , Fig. 11(b). Evidence of ridge formation was also observed at higher particle concentrations, Fig. 11(c-d).

4. Discussion

4.1 Effect of applied load and particle concentration on the abrasion, corrosion and abrasion-corrosion interactions

The results Fig. 7 , indicate a clear pattern of wear rate with load, with the micro-abrasion-corrosion rate peaking at intermediate loads. Such patterns have also seen in previous work by the current authors [13-14]where the transition to low wear at higher

loads was attributed to a transition to possible ridge formation and an abrasion-sliding wear transition, associated with oxidative wear as a result of formation of oxide at the contact interface.

It is interesting that there is some evidence of a shift in the maximum wear rate versus load curve, with changes in particle concentration, but the results are not consistent over all loads for the effect of this parameter. At low particle concentration levels, Fig. 7(a-c), the peak in the wear rate versus load shifts to lower loads with increasing particle concentration. At higher particle concentrations, the reverse is observed, with the wear rate versus load peak shifting to higher loads with increasing particle concentration, Fig. 7(d-e). The reasons for such behaviour are unclear at present but suggest the tribo-chemical mechanism at higher loads may be altering the wear mechanism.

The polarization data, Fig. 8-9, clearly indicates that Ti passivates in such conditions. The data indicates that the zero current potential shifts to lower values for increasing load and particle concentration, thus suggesting that passivity is reduced with increasing load and concentration. The evidence of transpassivation at more anodic potentials is interesting as it identifies an important change in the corrosion mechanism at higher potentials and that the film on the Titanium is no longer stable in such conditions.

The morphological features of the wear scar, Figs. 10-11, show classic micro-abrasion features, ridge formation and the presence of wear debris. Evidence of a polishing action at higher loads, Fig. 11(b), is indicative of a possible transition to an oxidative wear mechanism, where frictional heating at the contact results in an increase in the oxidation rate. This has also been observed in other work [13].

4.2 Construction of micro-abrasion-corrosion maps

A new approach by the current authors is to construct mechanistic maps, charting the transitions between the bio-tribo-corrosion regimes as a function of the main tribo-corrosion parameters [9]. This enables the following analysis to be carried out:

(i) Identification of mode of degradation i.e. whether the surface is immune from corrosion, whether it dissolves or passivates in the aqueous environment.

(ii) Establishment of the level of wastage rate and potential "safe" and "unsafe" windows of operating conditions

(iii) Clarification of mode of tribo-corrosions i.e. whether "additive", synergistic or antagonistic bio-tribo-corrosion behavior occurs over the component.

Thus, such diagrams may assist in identifying the stages in the bio-tribological lifecycle for total joint replacements.

In this study, the important effect of particle concentration is assessed together with the effects of increasing applied load. This enables a simulation of the effects of increasing particle concentration at the contact. An increase in particle concentration in the contact is likely to arise due to wear of the implant material. Hence, such maps have practical significance in identifying limits to performance of implant materials.

Thus, a series of bio-tribo-corrosion maps, Fig. 12, have been constructed using such results from the following analysis.

All the regimes and mechanisms are plotted into maps and the data used to construct such maps is given in Table 3.

$Wa/Wc \leq 0.1$	Corrosion dominated	(3)
$0.1 < Wa/Wc \leq 1$	Corrosion-micro-abrasion dominated	(4)
$1 < Wa/Wc \leq 10$	Micro-abrasion-corrosion dominated	(5)
$Wa/Wc > 10$	Micro-abrasion dominated	(6)

The results, Fig. 12 (a), indicate that at high concentrations at intermediate loads, micro-abrasion dominates. At higher loads, and lower particle concenatrions, corrosion-micro-abrasion

dominates, thus indicating that at lower particle concentrations, corrosion is more dominant than abrasion on the map.

At intermediate concentrations, there is a transition to micro-abrasion dominated behaviour at higher loads, and at above this low particle concentration, at such loads a transition to micro-abrasion-corrosion. Such patterns are consistent with the results on the effect of load and particle concentration, Fig. 7, where the effects at various load ranges tended to be different.

A map can also be constructed to identify zones of low and high wastage, i.e. .

$Wac \leq 3 . 10^{-6}g$ Low (7)

$3 . 10^{-6}g < Wac \leq 6 . 10^{-6}g$ Medium (8)$Wac > 6 . 10^{-6}g$ High (9)

Here, Fig. 12(b), there is a clear region of high wastage at low loads and high concentrations, with the low region dominating the map, in the low particle concentration range. Comparing the mechanism map, Fig. 12(a), with the wastage map, Fig. 12(b), suggests the wastage is highest where corrosion is significantly less i.e. the micro-abrasion-dominated regime, at high particle concentrations and intermediate loads and identifies how the effects of particle concentration are critically dependent on applied load.

If the values of Wa and Wc are further sub-divided as in earlier work [15-16]:

i.e. $Wa = \Delta Wa + Wao$ (10)

and $Wc = \Delta Wc + Wco$ (11)

then we can construct a methodology for identifying the various synergies between the processes.

$\Delta Wa/\Delta Wc \leq 0.1$	Additive	(12)
$1 \geq \Delta Wa/\Delta Wc > 0.1$	Additive-Synergistic	(13)
$\Delta Wa/\Delta Wc > 1$	Synergistic	(14)

It is shown, Fig. 12(c), on the synergy map that synergistic effects are associated with the high particle concentrations and loads and overlap the boundaries of medium and high wastage in Fig. 12(b). The synergistic effect defines the positive change in wear as a result of corrosion. This map indicates that as the synergistic region occupies the largest area at higher loads, and as corrosion is also more dominant in such conditions, tribo-chemical effects are likely to play an important effect in such conditions, to a greater extent than at lower loads, and this is possibly due to frictional heating effects on the surface of the material.

The results are interesting in that they show, that in such conditions, unlike the behaviour observed for Co-Cr in Ringer's solution [9], the film on the surface does not provide protection during abrasion and is removed (In the latter case, the behaviour was found to be antagonistic- i.e. displaying negative synergism). This may be due to the fact the Titanium Oxide formed on the surface in the Hank's solution is less resistant to wear than the Chromium Oxide formed on the Co-Cr material in the Ringer's solution evaluated in previous work[9]. For the implant material, the potential at which it will rest will depend on the level of activity of the individual

and the applied load determined by the body mass. If such a window of conditions can be identified for patient/activity levels, optimum replacement joint materials may defined for individual patients, and furthermore, performance limits may be generated for implant of various materials exposed to simulated body fluids.

Clearly, the bio-tribo-corrosion map is an important new technique for assessing tribo-corrosion of implant materials. Recent work on the tribo-corrosion of dental materials has shown the potential application of such maps to optimizing dental materials. [17]. Further work will be to investigate the behaviour of Ti in other solutions in addition to modelling the transition boundaries for such materials in such conditions.

5. Conclusions

(i) Micro-abrasion-corrosion experiments on Ti in Hanks solution indicated that the wear rate is dependent on load and particle concentration, with various maxima observed for the wear rate as a function of load. The loads where such maxima were observed were dependent on the particle concentration.

(ii) There was clear evidence that the corrosion contribution to the wear rate reduced significant at the higher loads and particle concentrations of the test environments

(iii) Micro-abrasion-corrosion maps have been constructed showing the degradation mechanism, level and extent of synergy over the material.

6. References

1. *The adult hip*, J. J. Callaghan, A.G. Rosenberg, H.E Rubash, Lippincott, Williams and Wilkins, 2nd Ed, Philadelphia, USA, 2007.
2. S.C. Lim, M.F. Ashby, J.H. Brunton, "Wear-rate transitions and their relationship to wear mechanisms", Acta Metallurgica, Volume 35, Issue 6, June 1987, Pages 1343-1348
3. G. Sundararajan, "An analysis of the erosion-oxidation interaction mechanisms" Wear, Volume 145, Issue 2, 21 May 1991, Pages 251-282
4. M. M. Stack, B. D. Jana , Modelling particulate erosion–corrosion in aqueous slurries: some views on the construction of erosion–corrosion maps for a range of pure metals Wear, Volume 256, Issues 9-10, May 2004, Pages 986-1004
5. M.M. Stack, S.M. Abdelrahman, B.D. Jana, " A new methodology for modelling erosion–corrosion regimes on real surfaces: Gliding down the galvanic series for a range of metal-corrosion systems,Wear, Volume 268, Issues 3-4, 4 February 2010, Pages 533-542
6. M.M. Stack and T.M. Abd El Badia, (2008) "Some comments on mapping the combined effects of slurry concentration, impact velocity and electrochemical potential on the erosion-corrosion of WC/Co-Cr, *Wear*, 264, 826-837.
7. M.M. Stack and G.H. Abdulrahman, (2010)"Mapping erosion-corrosion of carbon steel in oil exploration conditions: Some new approaches to characterizing mechanisms and synergies", *Tribology International,* 43, 7, 1268-1277.
8. M Pourbaix, Atlas of Electrochemical Equilibria in Aqueous Solution, 1974, NACE
9. M.M. Stack, J. Rodling, M.T. Mathew, H. Jawan, W. Huang, G. Park, C. Hodge "Micro-abrasion - corrosion of a Co-Cr/UHMWPE couple in Ringer's solution: an approach to

construction of mechanism and synergism maps for application to bio-implants" *Wear*, 269, 5-6, 376-382.

10. R . Büscher and A. Fischer, "Metallurgical Aspects of Sliding Wear of FCC Materials for Medical Applications", (2003). *Materialwissenscgaft und Werkstofftechnik*, 34, 966.
11. D. Sun, J.A. Wharton, R.J.K. Wood, and W.M. Rainforth, (2009), "Microabrasion-corrosion of cast CoCrMo alloy in simulated body fluids". *Tribology International*, 42, (1), 99-110.
12. I.M. Hutchings and K.L. Rutherford, (1997),"Theory and Application of a Micro-Scale Abrasive Wear Test". *J Test Eval*, *JTEVA*, 25(2), 250-260.
13. M.M Stack M. M., Mathew., (2003),"Micro-abrasion transitions of metallic materials", *Wear*, 255 (1-6), 14-22.
14. M. M. Stack , H. Jawan and M.T. Mathew, (2005), "On the construction of micro-abrasion maps for a Steel/Polymer couple in corrosive environments", *Tribology International*, 38 (9), 848-856.
15. M.M. Stack and T.M Abd El Badia (2006),"On the construction of erosion-corrosion maps for WC/Co-Cr- based coatings in aqueous conditions", *Wear*, 261 (11-12), 1181-1190.
16. Z. Yue, P. Zhou, J. Shi, In: K. C. Luedema, editor.(1987) *Proceedings of conference on wear of materials*. New York:ASME:.763-768.
17. Hsin-Chun Wang, M. M. Stack, Ting-Fu Hong, Moo-Chin Wang, Wang-Long Li ,(2010) On the construction of wear maps for Y-TZP dental ceramics in aqueous environments: pH, exposure time and impact angle effects", *Tribology International* (in press) doi:10.1016/j.triboint.2010.06.015

7. Captions for tables

1. Specification of micro-abrasion apparatus
2. Composition of TLM alloy
3. Mechanical properties of TLM alloy
4. Experimental details
5. Values of micro-abrasion, corrosion and micro-abrasion-corrosion contributions.

8. Captions for figures

1. Experimental apparatus for micro-abrasion tests

2. SEM of specimens prior to exposure

3. SEM of SiC particles

4. Effect of slurry concentration on on friction coefficient

   (a) 0.25 N

   (b) 0.5 N

   (c) 1.0 N

   (d) 2.0N

5. Effect of applied load on friction coefficient

   (a) 0.025 g cm^{-3}

   (b) 0.05 g cm^{-3}

   (c) 0.1 g cm^{-3}

   (d) 0.2 g cm^{-3}

   (a) 0.25 g cm^{-3}

6. Variation of wear volume with sliding distance and slurry concentration

7. Variation of Wac, Wa and Wc with load

(a) 0.025 g cm^{-3}

(b) 0.05 g cm^{-3}

(c) 0.1 g cm^{-3}

(d) 0.2 g cm^{-3}

(a) 0.25 g cm^{-3}

8. Polarization data at various loads

(a) 0.025 g cm^{-3}

(b) 0.05 g cm^{-3}

(c) 0.1 g cm^{-3}

(d) 0.2 g cm^{-3}

(a) 0.25 g cm^{-3}

9. Polarization data at various concentrations

(a) 0.25 N

(b) 0.5 N

(c) 1.0 N

(d) 2.0N

10. SEM of morphologies following exposure at 0.2 g cm-3 and sliding distance of 89.73 m

(a) 0.25 N

(b) 0.25 N at higher magnification

© 1 N

(d) 1N at higher magnification

11. SEM of morphologies following exposure at 1N and sliding distance of 149.54 m

(a)Concentration of 0.1 g cm^{-3}

(b) Higher magnification of (a)

© Concentration of 0.2g cm^{-3}

(d) Concentration of 0.25 g cm^{-3}

12. Micro-abrasion-corrosion map

(a) Mechanism map

(b) Wastage map

© Synergy map

Table 1

Model	TE-66
Supplier	Phoenix tribology (Plint), UK.
Load range	0.025 to 5 N
Ball diameter	25 mm
Ball speed range	30 - 150 rpm
Pump feed rate	To 1 ml s^{-1} (Based on 0.5mm bore)

Table2

Material	Ti	Mo	Zr	Nb	N	H	Sn	O	C	Fe
TLM	bal.	2.90	3.08	25.1	0.03	0.003	2.02	0.14	0.01	0.03

Table 3

Material	Rm/MPa	Rp/MPa	Z/%	H/ HV	E/GPa	A/%
TLM	960	915.77	12.42	235	79.4	5.75

Table 4

Sample material	Ti alloy
Ball material	Zirconia
Speed	100 rpm
Load	0.25-2 N
Sliding distance	89.37 and 149.54 m
Conditions	Cncentration of SiC 0.025-0.25 g cm-3

Slurry	Hanks solution mixed with SiC particles 2.2 Hank's solution: 50mL C+ 50mL D+ 24mL E+900mLH_2O + $CHCl_3$; C：160gNaCl+8g KCl+4g $MgSO_4 \cdot 7H_2O$+2.8g $CaCl_2$+1L H_2O ; D：1.2g $Na_2HPO_4 \cdot 7H_2O$+2.0g$NaH_2PO_4 \cdot H_2O$+20.0g$C_6H_{12}O_6$+1L H_2O ; E：7g $NaHCO_3$+500mL H_2O ; **pH = 7.2 ~ 7.8**

Table 5

SC (g/cm^3)	Load (N)	Wac (g)	Wc (g)	Wa (g)	Wao (g)	Wco (g)	△Wa (g)	Wc/Wa
0.025	0.25	2.53E-05	5.58E-06	1.97E-05	4.17E-07	8.56E-08	1.93E-05	0.283012
	0.5	1.80E-05	5.69E-06	1.23E-05	1.32E-06	8.56E-08	1.10E-05	0.461650
	1	2.06E-05	1.53E-05	5.27E-06	9.46E-07	8.56E-08	4.32E-06	2.907220
	2	2.33E-05	1.30E-05	1.03E-05	2.35E-06	8.56E-08	7.99E-06	1.256816
0.05	0.25	2.70E-05	1.51E-06	2.55E-05	4.89E-06	8.56E-08	2.06E-05	0.059210
	0.5	3.24E-05	3.84E-06	2.85E-05	4.32E-06	8.56E-08	2.42E-05	0.134489
	1	2.83E-05	1.32E-05	1.51E-05	2.07E-06	8.56E-08	1.31E-05	0.872811
	2	1.70E-05	1.62E-06	1.54E-05	3.76E-06	8.56E-08	1.16E-05	0.105132
0.1	0.25	7.53E-05	5.00E-05	2.52E-05	1.22E-05	8.56E-08	1.30E-05	1.983691
	0.5	7.45E-05	3.33E-05	4.12E-05	1.09E-05	8.56E-08	3.03E-05	0.807699

	1	6.17E-05	3.43E-05	2.74E-05	9.82E-06	8.56E-08	1.76E-05	1.253102
	2	6.68E-05	7.29E-07	6.61E-05	8.84E-06	8.56E-08	5.73E-05	0.011031
	0.25	8.78E-05	4.83E-06	8.30E-05	4.55E-05	8.56E-08	3.75E-05	0.058165
	0.5	1.08E-04	3.71E-06	1.04E-04	4.20E-05	8.56E-08	6.22E-05	0.035556
0.2	1	7.75E-05	3.00E-06	7.45E-05	2.79E-05	8.56E-08	4.66E-05	0.040333
	2	3.67E-05	4.45E-06	3.23E-05	2.41E-05	8.56E-08	8.17E-06	0.137771
	0.25	9.51E-05	5.87E-06	8.92E-05	8.64E-05	8.56E-08	2.81E-06	0.065788
	0.5	1.61E-04	8.53E-06	1.52E-04	9.85E-05	8.56E-08	5.39E-05	0.055996
0.25	1	1.64E-04	6.08E-06	1.58E-04	1.24E-04	8.56E-08	3.43E-05	0.038399
	2	6.63E-05	8.27E-06	5.81E-05	1.71E-05	8.56E-08	4.10E-05	0.142379

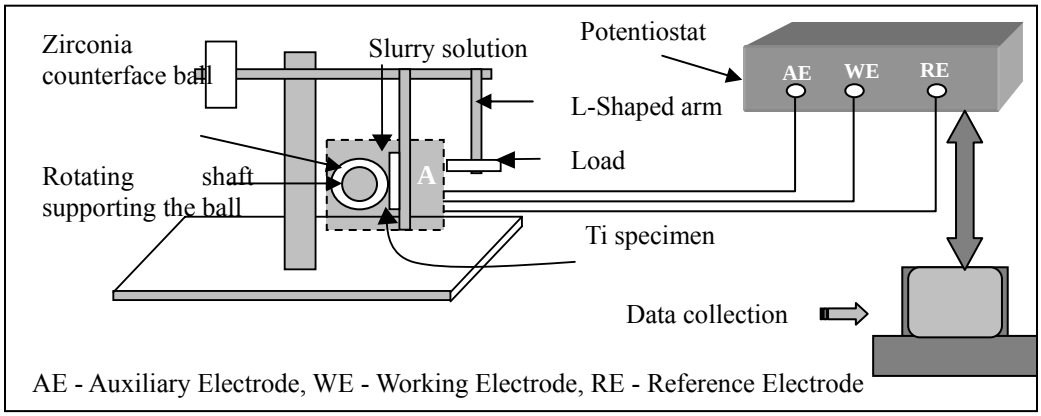
Zirconia
counterface ball
Slurry solution
Potentiostat
AE
WE
RE
L-Shaped arm
Load
Rotating shaft
supporting the ball
A
Ti specimen
Data collection
AE - Auxiliary Electrode, WE - Working Electrode, RE - Reference Electrode

Figure 1

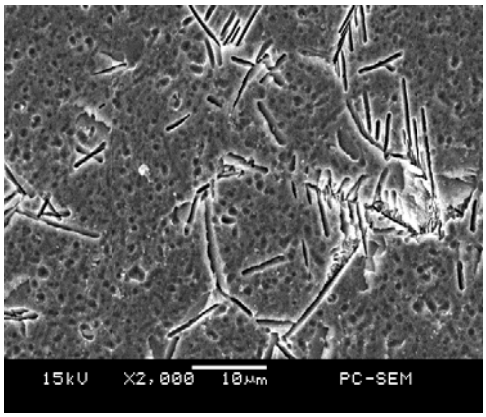

Fig. 2

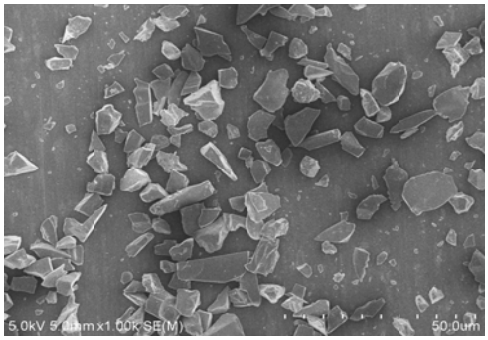

Fig. 3

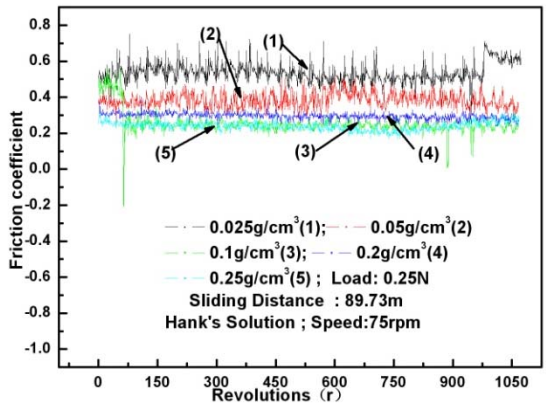

(a)

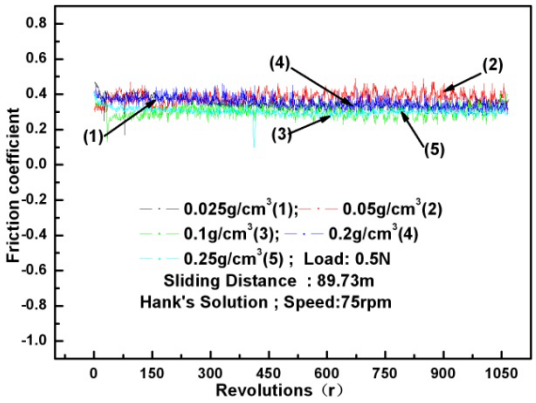

(b)

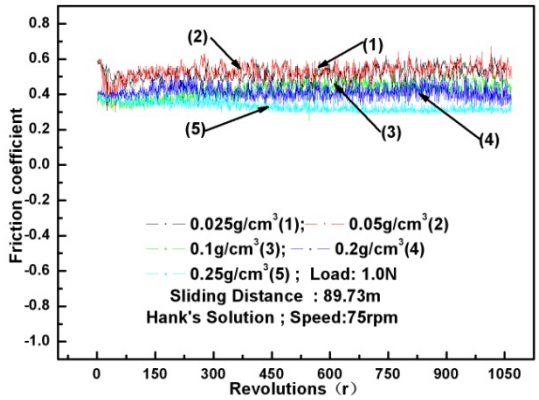

(c)

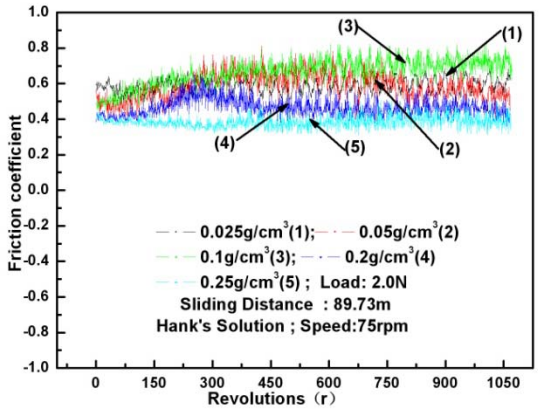

(d)

Figure 4

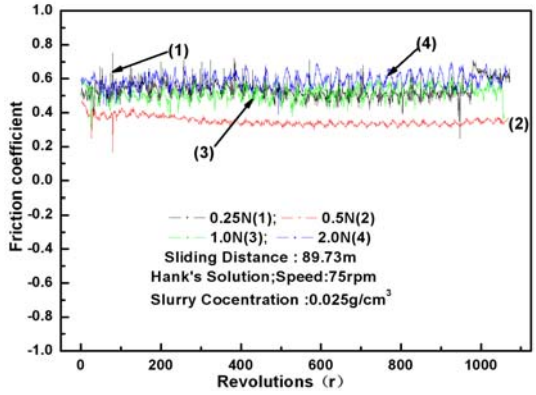
Friction coefficient
Revolutions（r）
(1)
(2)
(3)
(4)
0.25N(1); 0.5N(2)
1.0N(3); 2.0N(4)
Sliding Distance : 89.73m
Hank's Solution;Speed:75rpm
Slurry Cocentration :0.025g/cm3

(a)

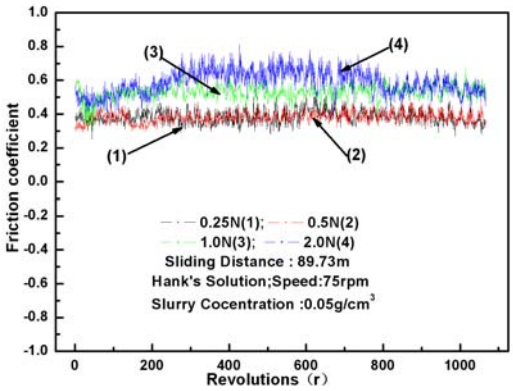
Friction coefficient
Revolutions（r）
(1)
(2)
(3)
(4)
0.25N(1); 0.5N(2)
1.0N(3); 2.0N(4)
Sliding Distance : 89.73m
Hank's Solution;Speed:75rpm
Slurry Cocentration :0.05g/cm3

(b)

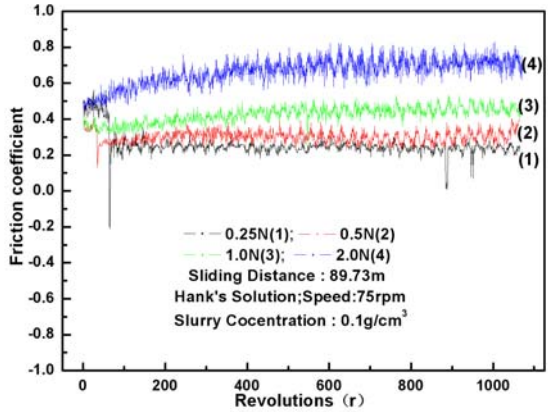
Friction coefficient
Revolutions（r）
(1)
(2)
(3)
(4)
0.25N(1); 0.5N(2)
1.0N(3); 2.0N(4)
Sliding Distance : 89.73m
Hank's Solution;Speed:75rpm
Slurry Cocentration : 0.1g/cm3

(c)

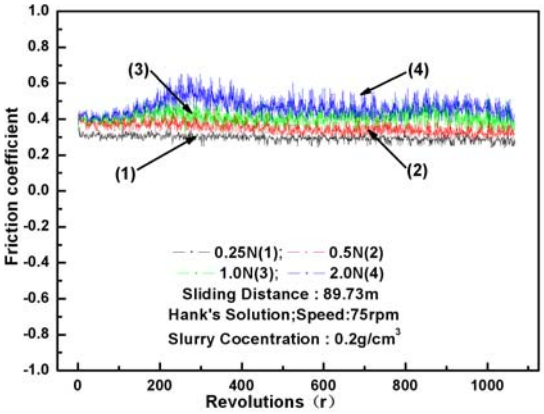
Friction coefficient
Revolutions（r）
(1)
(2)
(3)
(4)
0.25N(1); 0.5N(2)
1.0N(3); 2.0N(4)
Sliding Distance : 89.73m
Hank's Solution;Speed:75rpm
Slurry Cocentration : 0.2g/cm3

(d)

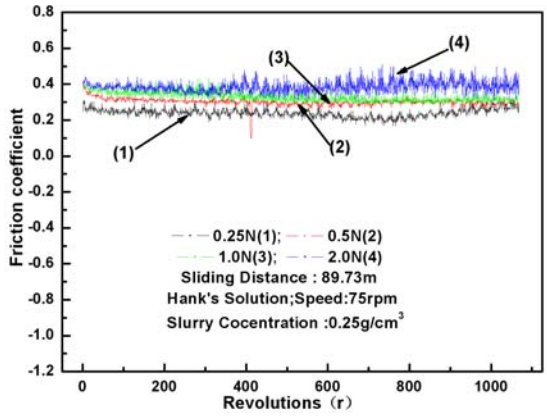
Friction coefficient
Revolutions（r）
(1)
(2)
(3)
(4)
0.25N(1); 0.5N(2)
1.0N(3); 2.0N(4)
Sliding Distance : 89.73m
Hank's Solution;Speed:75rpm
Slurry Cocentration :0.25g/cm3

(e)

Fig. 5

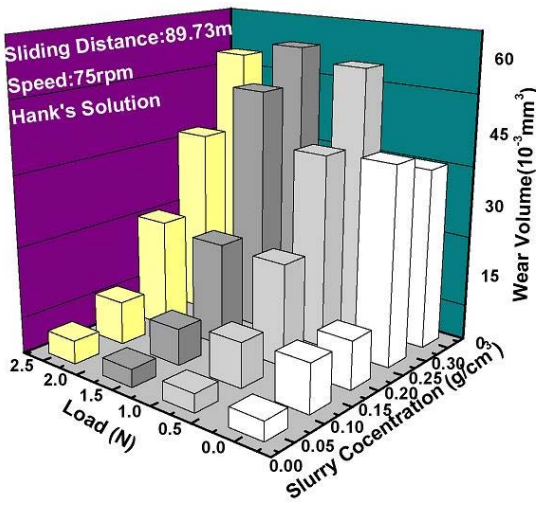
Sliding Distance:89.73m
Speed:75rpm
Hank's Solution
Load (N)
2.5
2.0
1.5
1.0
0.5
0.0
Slurry Cocentration (g/cm3)
0.00
0.05
0.10
0.15
0.20
0.25
0.30
Wear Volume(10-3mm3)
0
15
30
45
60

Fig. 6

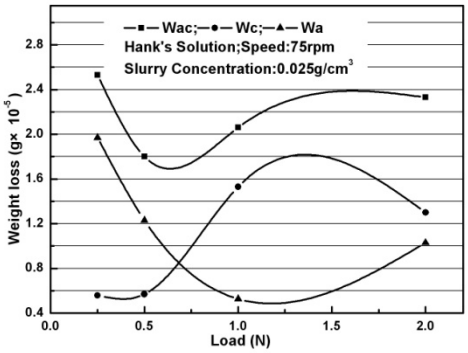
—■— Wac;—●— Wc;—▲— Wa
Hank's Solution;Speed:75rpm
Slurry Concentration:0.025g/cm3
Weight loss (g× 10-5)
Load (N)

(a)

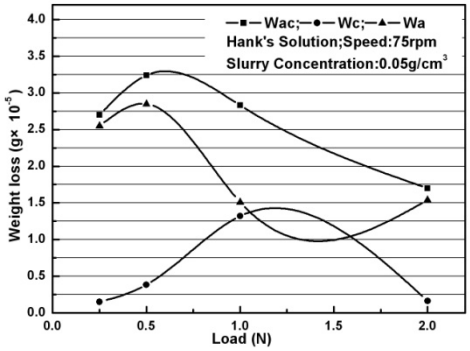
—■— Wac;—●— Wc;—▲— Wa
Hank's Solution;Speed:75rpm
Slurry Concentration:0.05g/cm3
Weight loss (g× 10-5)
Load (N)

(b)

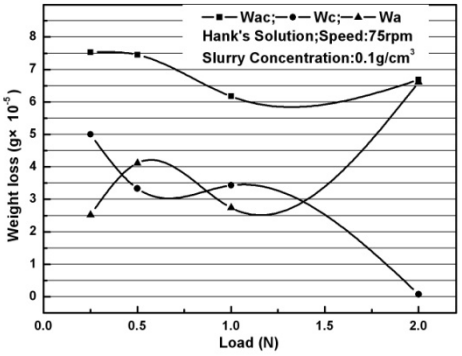
—■— Wac;—●— Wc;—▲— Wa
Hank's Solution;Speed:75rpm
Slurry Concentration:0.1g/cm3
Weight loss (g× 10-5)
Load (N)

(c)

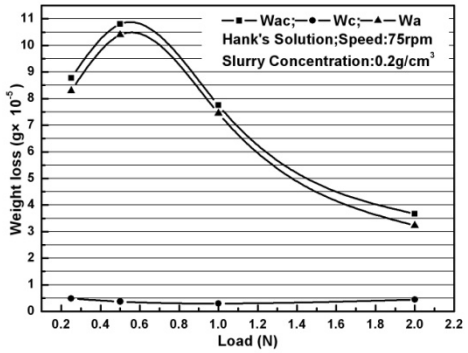
—■— Wac;—●— Wc;—▲— Wa
Hank's Solution;Speed:75rpm
Slurry Concentration:0.2g/cm3
Weight loss (g× 10-5)
Load (N)

(d)

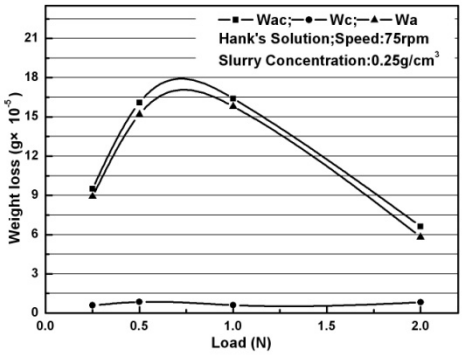
—■— Wac;—●— Wc;—▲— Wa
Hank's Solution;Speed:75rpm
Slurry Concentration:0.25g/cm3
Weight loss (g× 10-5)
Load (N)

(e)

Figure 7

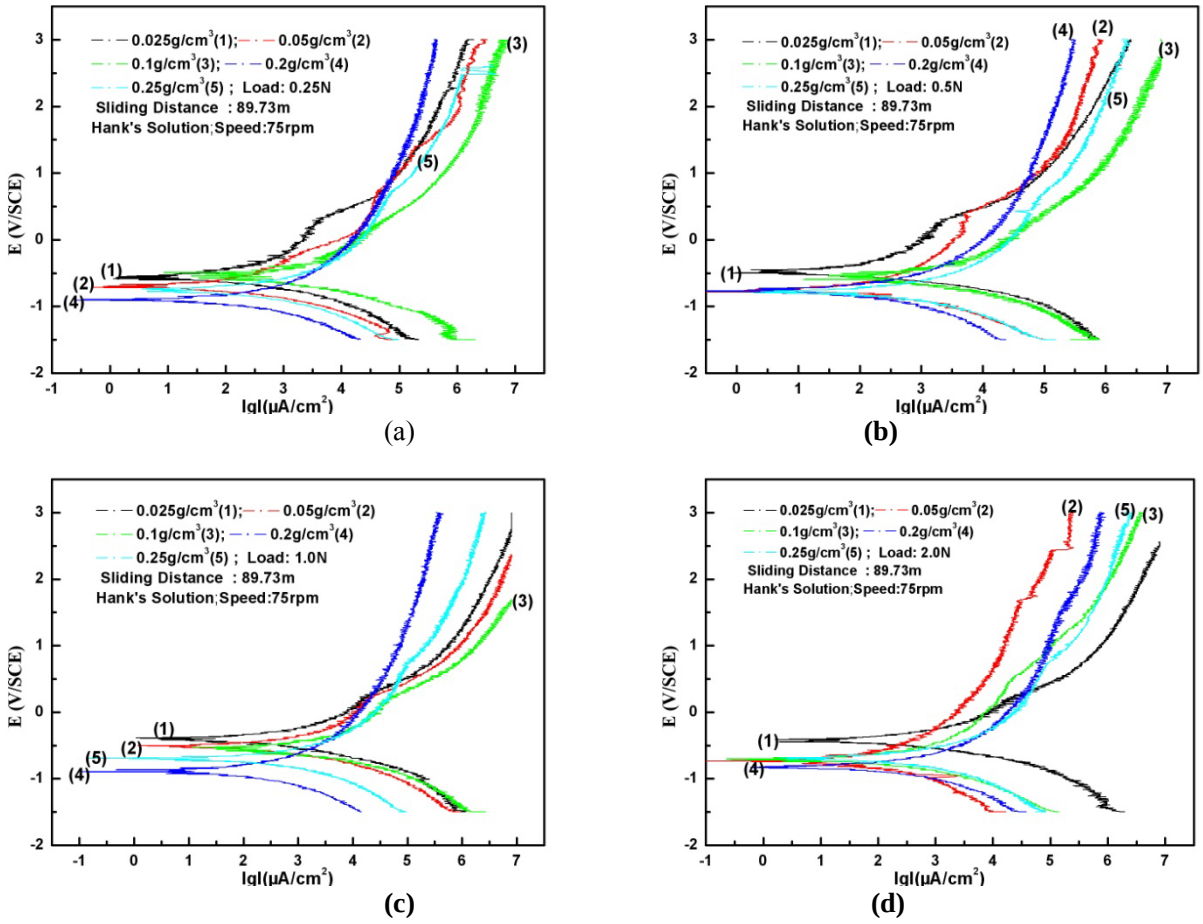
0.025g/cm3(1); 0.05g/cm3(2)
0.1g/cm3(3); 0.2g/cm3(4)
0.25g/cm3(5) ; Load: 0.25N
Sliding Distance : 89.73m
Hank's Solution;Speed:75rpm
E (V/SCE)
lgI(μA/cm2)
(a)
0.25g/cm3(5) ; Load: 0.5N
(b)
0.25g/cm3(5) ; Load: 1.0N
(c)
0.25g/cm3(5) ; Load: 2.0N
(d)

Figure 8

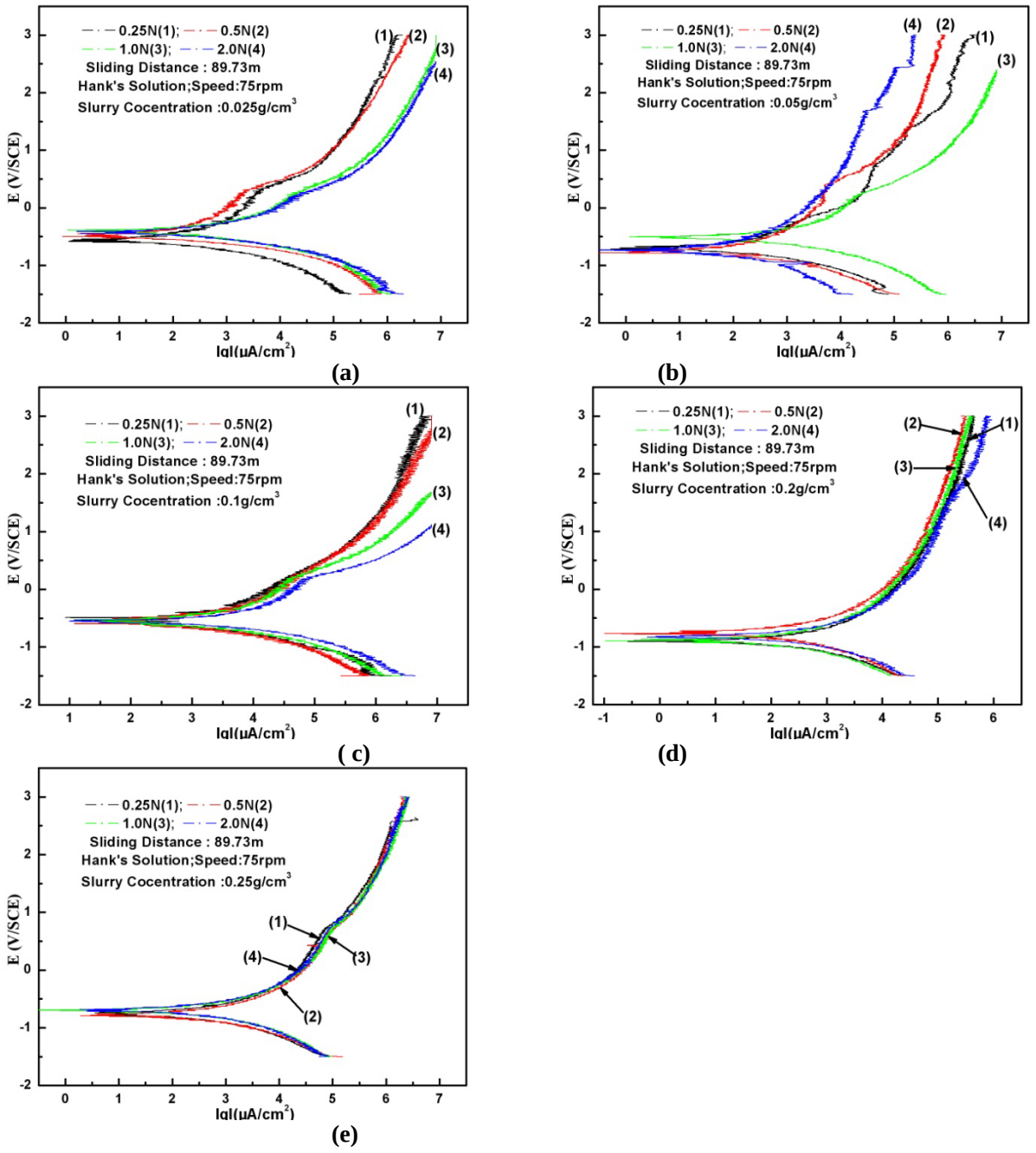
0.25N(1); 0.5N(2)
1.0N(3); 2.0N(4)
Sliding Distance : 89.73m
Hank's Solution;Speed:75rpm
Slurry Cocentration :0.025g/cm3
E (V/SCE)
lgI(μA/cm2)
(a)
Slurry Cocentration :0.05g/cm3
(b)
Slurry Cocentration :0.1g/cm3
(c)
Slurry Cocentration :0.2g/cm3
(d)
Slurry Cocentration :0.25g/cm3
(e)

Fig. 9

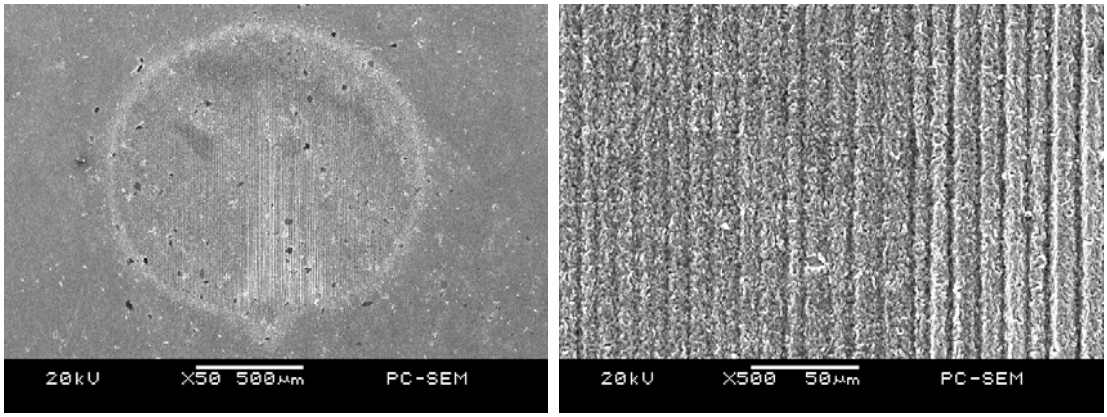

(a) (b)

(c)

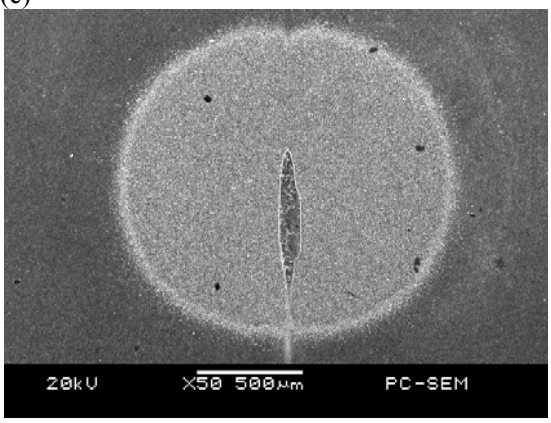

(d)

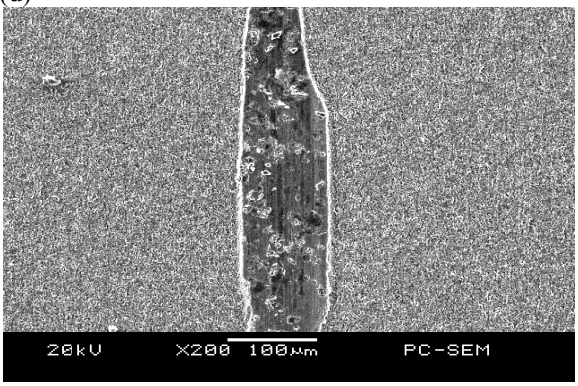

Figure 10.

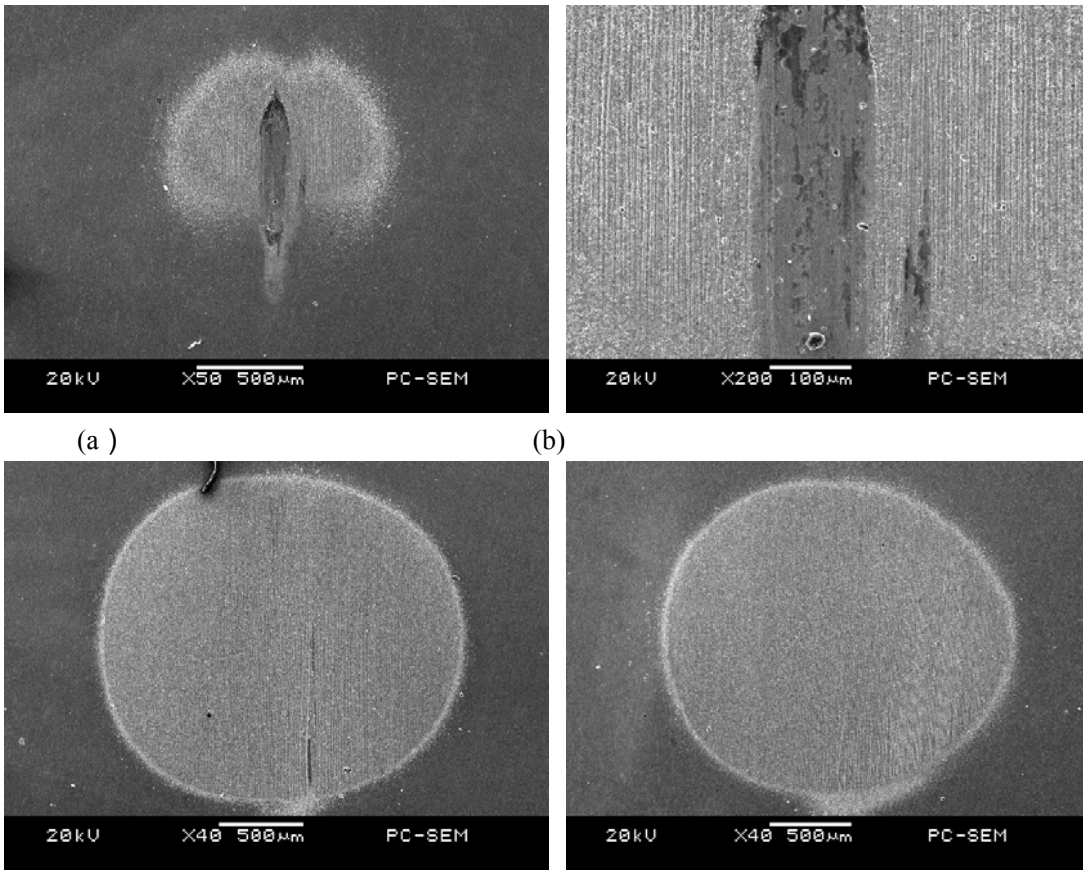
20kV X50 500µm PC-SEM
20kV X200 100µm PC-SEM
(a)
(b)
20kV X40 500µm PC-SEM
20kV X40 500µm PC-SEM
(c)
(d)

Figure 11

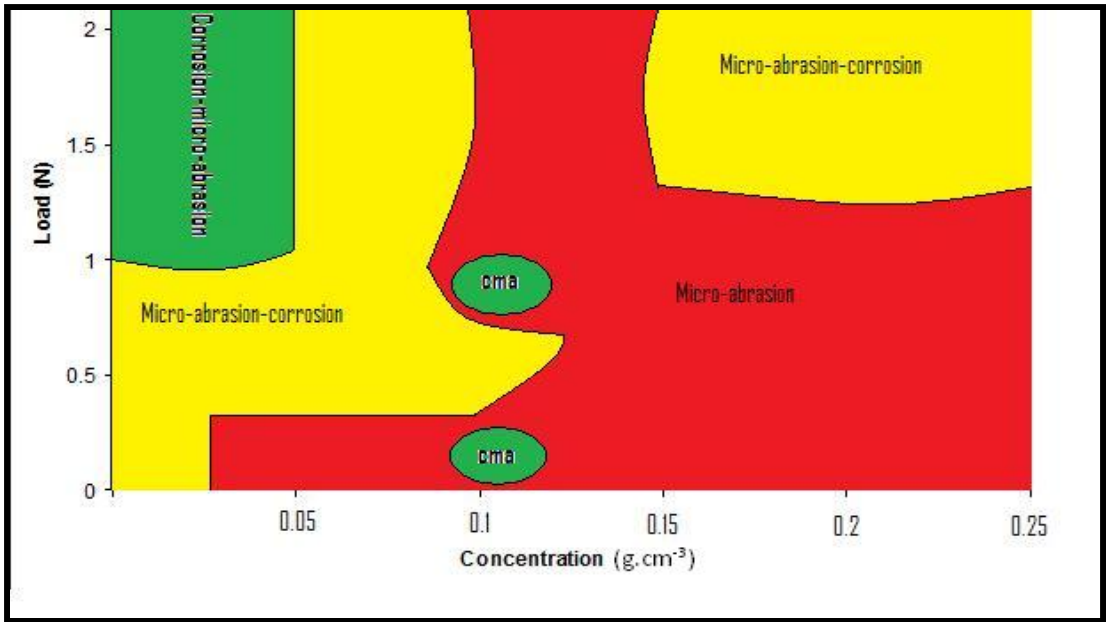
Corrosion-micro-abrasion
Micro-abrasion-corrosion
cma
Micro-abrasion
Micro-abrasion-corrosion
cma
Load (N)
Concentration (g.cm-3)
0
0.5
1
1.5
2
0.05
0.1
0.15
0.2
0.25

(a)

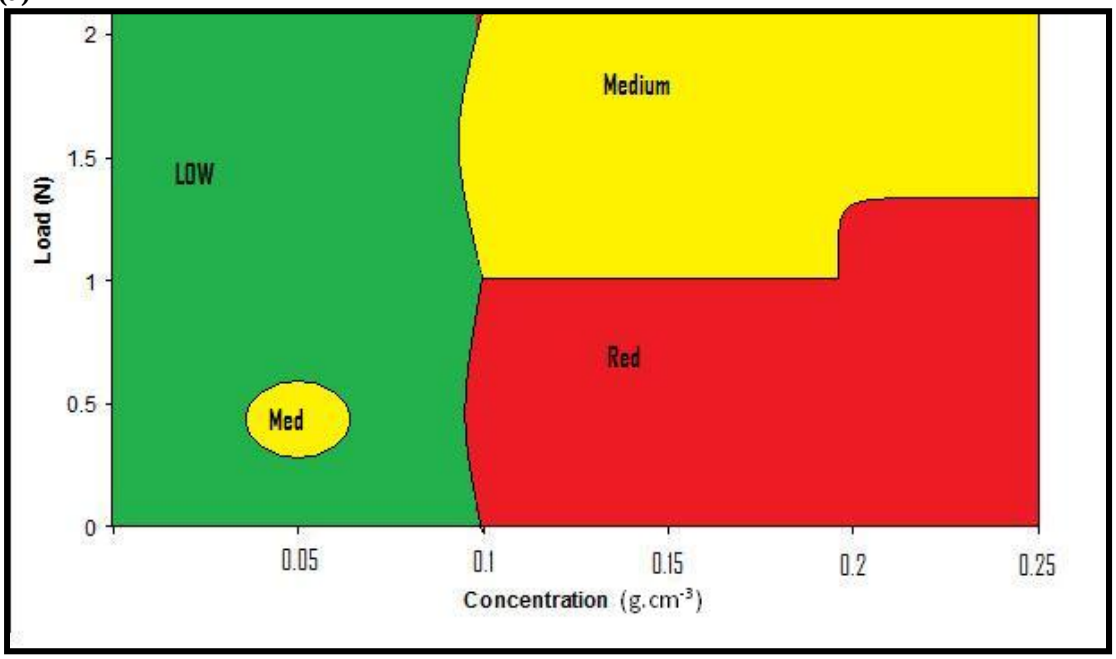
LOW
Medium
Red
Med
Load (N)
Concentration (g.cm-3)
0
0.5
1
1.5
2
0.05
0.1
0.15
0.2
0.25

(b)

Fig. 12

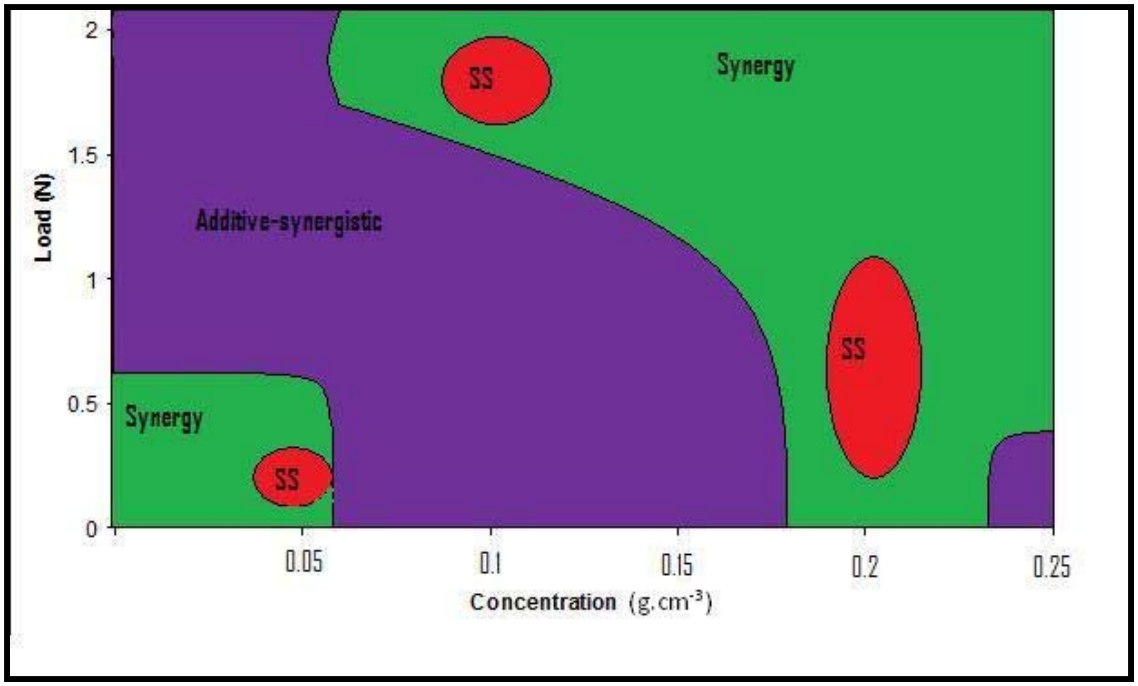
Load (N)
2
1.5
1
0.5
0
SS
Synergy
Additive-synergistic
SS
Synergy
SS
0.05
0.1
0.15
0.2
0.25
Concentration (g.cm-3)

Figure 12. (c)